Med Biol Eng Comput (2008) 46:1139–1152
DOI 10.1007/s11517-008-0377-0

SPECIAL ISSUE - ORIGINAL ARTICLE

Patient-specific surgical planning and hemodynamic computational fluid dynamics optimization through free-form haptic anatomy editing tool (SURGEM)

Kerem Pekkan · Brian Whited · Kirk Kanter · Shiva Sharma · Diane de Zelicourt · Kartik Sundareswaran · David Frakes · Jarek Rossignac · Ajit P. Yoganathan

Received: 23 January 2007 / Accepted: 13 July 2008 / Published online: 5 August 2008

Abstract The first version of an anatomy editing/surgical planning tool (SURGEM) targeting anatomical complexity and patient-specific computational fluid dynamics (CFD) analysis is presented. Novel three-dimensional (3D) shape editing concepts and human–shape interaction technologies have been integrated to facilitate interactive surgical morphology alterations, grid generation and CFD analysis. In order to implement "manual hemodynamic optimization" at the surgery planning phase for patients with congenital heart defects, these tools are applied to design and evaluate possible modifications of patient-specific anatomies. In this context, anatomies involve complex geometric topologies and tortuous 3D blood flow pathways with multiple inlets and outlets. These tools make it possible to freely deform the lumen surface and to bend and position baffles through real-time, direct manipulation of the 3D models with both hands, thus eliminating the tedious and time-consuming phase of entering the desired geometry using traditional computer-aided design (CAD) systems. The 3D models of the modified anatomies are seamlessly exported and meshed for patient-specific CFD analysis. Free-formed anatomical modifications are quantified using an in-house skeletization based cross-sectional geometry analysis tool. Hemodynamic performance of the systematically modified anatomies is compared with the original anatomy using CFD. CFD results showed the relative importance of the various surgically created features such as pouch size, vena cave to pulmonary artery (PA) flare and PA stenosis. An interactive surgical-patch size estimator is also introduced. The combined design/analysis cycle time is used for comparing and optimizing surgical plans and improvements are tabulated. The reduced cost of patient-specific shape design and analysis process, made it possible to envision large clinical studies to assess the validity of predictive patient-specific CFD simulations. In this paper, model anatomical design studies are performed on a total of eight different complex patient specific anatomies. Using SURGEM, more than 30 new anatomical designs (or candidate configurations) are created, and the corresponding user times presented. CFD performances for eight of these candidate configurations are also presented.

Electronic supplementary material The online version of this article (doi:10.1007/s11517-008-0377-0) contains supplementary material, which is available to authorized users.

K. Pekkan (✉)
Biomedical Engineering, Carnegie Mellon University,
Pittsburgh, PA, USA
e-mail: kpekkan@andrew.cmu.edu

B. Whited · J. Rossignac
College of Computing,
Georgia Institute of Technology,
Atlanta, GA, USA

K. Kanter
Department of Cardiothoracic Surgery,
Emory University School of Medicine,
Atlanta, GA, USA

S. Sharma
Pediatric Cardiology Associates, Atlanta, GA, USA

D. de Zelicourt · K. Sundareswaran · A. P. Yoganathan
Wallace H. Coulter Department of Biomedical Engineering,
Georgia Institute of Technology and Emory University School
of Medicine, Room 2119 U.A. Whitaker Building,
313 Ferst Dr., Atlanta, GA 30332-0535, USA

D. Frakes
Harrington Department of Bioengineering and Electrical
Engineering, Arizona State University, Tempe, AR, USA

Keywords Patient specific surgical planning · Computational fluid dynamics · Congenital heart defects · Computer aided design

1 Introduction

Complex reconstructive cardiovascular surgeries are performed in patients having congenital heart a defect (about 2,000 babies in a year in the US) in which there is only one effective pumping chamber. Depending on the lesion three stages of surgeries are required to enable right-heart bypass and transition to the single-ventricle circulation. Earlier studies have demonstrated that the geometric configuration of the surgical repair site is a primary factor in determining the hemodynamic efficiency of the connection and in turn, could influence postoperative outcomes [5, 7, 8, 10, 29, 44] and cardiac output [46, 70, 71]. A recent study showed that there is still room for hemodynamic improvement (up to 40%) over the current "best" Fontan surgical pathways [60]. To improve patient's health, cardiovascular pre-surgical planning and blood flow optimization before the in vivo execution at the operating room is the logical process for the engineer (Fig. 1). The three pillars of this technology are (1) image-based computational fluid dynamics (CFD) analysis; (2) anatomical editing—geometrical human–shape interaction; and (3) the exchange of 3D geometrical information between the patient's data, the surgeon, CFD analysis and numerical optimization.

Image-guided surgery and surgical planning is routinely being applied in neurosurgery, spine surgery, abdominal surgery, and orthopedic surgery [1, 2, 15, 55, 74]. Recently, with advancements in computational fluid dynamics simulation technologies, surgical planning is being applied to the cardiovascular system [16, 31, 32, 51, 52, 54, 64–67, 80]. For example, Taylor et al. have attempted surgical planning for aorta-illiac occlusive disease by incorporating fast CFD solvers with 3D modeling using MRI [62, 63]. Steinman et al. have attempted similar planning techniques towards the detection and removal of atherosclerotic plaques using unsteady pulsatile CFD simulations with geometries and boundary conditions prescribed using patient-specific MRI [64–67]. Similar methods were applied to other cardiovascular systems such as the abdominal aortic aneurism [16, 31, 32, 54, 80] endovascular grafts [16, 20], pediatrics [19, 30], coronary arteries [51, 52], and congenital heart diseases [39, 40]. However, all of these studies primarily utilize surgical planning methods towards *analysis* of a limited number of anatomical geometries, and no one to date has used such methods towards *systematic geometric optimization* by combining MRI and CFD.

Recently our group has embarked upon attempting surgical planning by virtually modifying and optimizing geometries using CAD tools and simulating flow using CFD [6, 45, 47]. CFD tools are employed to answer clinical questions by altering the 3D cardiac magnetic resonance (CMR) anatomy model without in vivo execution. Anatomical modifications include virtual pulmonary artery angioplasty or fenestration [47], and for a bilateral superior vena cava (SVC) Fontan, the virtual inferior vena cava (IVC) location modification aimed at better perfusion at the PA segment bounded by the two SVCs [6]. Similarly, Migliavacca et al. [41] compared four alternative IVC geometries for a given Glenn stage anatomy (pre-surgery stage) and reported associated performance differences in

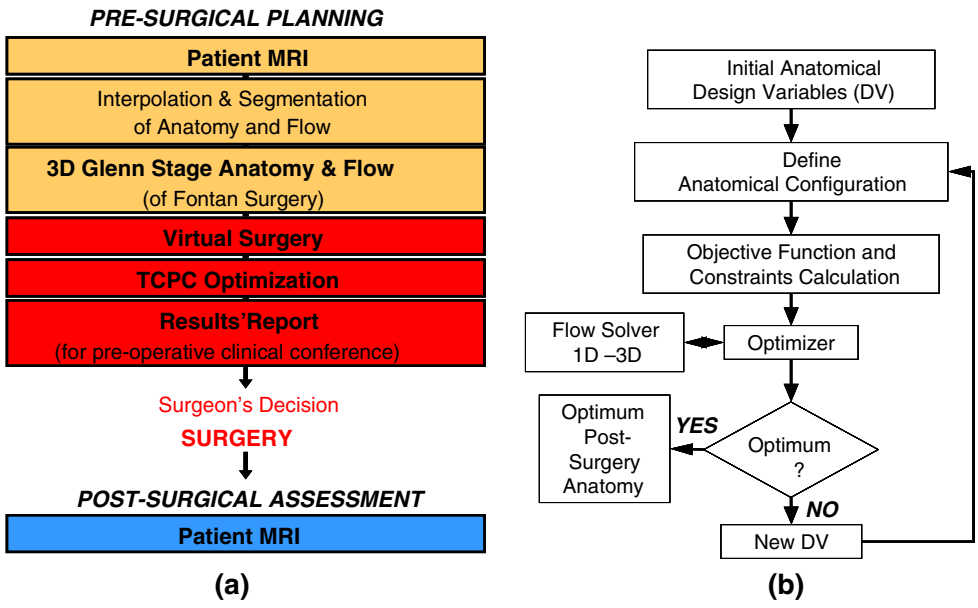

Fig. 1 **a** Surgical planning flowchart for Fontan (TCPC) surgeries. Hemodynamic TCPC optimization step in (**a**) can be performed on a number of candidate anatomies or through an automated process as shown in (**b**) which starts with an initial candidate anatomy and approaches to a local optima. (Glenn stage corresponds to the second palliative surgical operation which is also the pre-surgery stage for the third stage reconstruction)

their pulsatile CFD simulations. While these operations were conceptually and geometrically simple (uniform dilatation and linear IVC translation), realizing these in the computer medium with the state-of-the art commercial CAD systems, introduced enormous difficulties due to the complex, highly variable morphologies [26]. Unlike the perfect and uniform geometrical shapes designed in many traditional engineering CAD and computer-aided manufacturing applications, vascular anatomies are patient-specific and cannot be easily constructed as combinations of a small number of mathematically simple shape primitives or created by a sequence of digital counterparts of manufacturing operations [22]. Recent polyhedral modeling paradigms [9, 38] and related commercial tools that are developed particularly for inverse engineering design [81] and animation [82] can address the geometric complexity and offer considerable help in patient-specific applications. Still these current tools lack shape interaction, robust morphing and the requirement for manual building of the complete anatomy from polygonal primitives is not practical for all applications.

Therefore, the need for a general systematic framework that robustly handles any anatomical shape/complexity to address the demanding needs of cardiovascular surgery planning and assessment has emerged *naturally* as a conclusion of these earlier studies. In addition, to being an important building block of the clinical patient-specific methodology (from CMR to CFD), we believe that such a framework also lays the foundation for future fully *automated optimization* or *inverse design* studies of surgical pathways which have been overlooked in literature primarily due the anatomical complexity and very large parametric search space.

In this manuscript the first version of a human–shape interaction system, called SURGEM that is based on two-hand, free-form manipulation is described. We report its applications to the surgery planning and hemodynamic analysis of complex congenital heart defects. The shape-editing technologies is harnessed to remove the design bottleneck and in the future could bring the computer-aided pre-surgical patient-specific outcome assessment to its next level of effectiveness, enabling its practical clinical use and advance the current surgical decision making process for the benefit of patients.

2 Cardiovascular anatomical design and human–shape interaction

Shape interaction framework required for hemodynamic surgical planning can be established on a typical haptic hardware [25, 28] but for this application there is no need for sense feed-back or stereo displays. Free-form CAD surfaces are not necessarily associated with a closed-form mathematical definition and created through artistic/sculpturing [4, 36, 73] or reverse engineering measurements [75] of random point clouds. This open framework also allow for morphing [11, 18] and direct manipulation of surfaces through a limited number of intuitive parameters. Arbitrary surfaces and forms usually encountered in biomedical applications [33, 37, 59, 72] particularly suitable for the application of free-form computer graphics technologies. To the authors knowledge the most relevant work is performed by Quin et al. using a 3D motion capture system for free-form designing of a large-sized surfaces defined by a network of splines [53]. In addition recent, scene based, cardiovascular applications are also reported [34, 61]. Shape interaction tools that are employed in this manuscript target the integration of 3D free-form vascular vessel surface modifications with the fluid dynamic performance.

The real-time shape editing capabilities of SURGEM are based on a mathematical model of free-form deformations (FFD) that are weighted averages of pose-interpolating screw motions [23, 24], originally developed for editing motions that interpolate user-specified position and orientation constraints. This in-house mathematical tool is integrated with a new human–shape interaction methodology that uses two commercially available six degrees of freedom (DoF) trackers to control the parameters of the FFD by simple and natural gestures of both hands [35, 36, 83].

The starting point of the underlying technology stems from an attempt to produce a tool for virtual sculpturing. The idea is to let the user grab a portion of the shape and then pull, push, twist, and bend it (Fig. 2). Only the portion of the shape in the vicinity of the grabbed point is affected. The effect is lessened with distance through a specified decay profile.

Mathematical model of the warp is intuitive and effective for shape editing. Each hand manipulates a tracker that records 6 DoF (3 coordinates for position and 3 angles of rotation). Hence, each tracker tracks a coordinate system (or *pose*). When the user presses a button of the tracker, the left and right starting poses (S_L and S_R) are recorded. Current positions of the trackers define end poses (E_L and E_R). End poses change during manipulation (until the button is released). During shape editing, at each frame, a space warp (W) is computed and applied that satisfies these 12 position and orientation constraints simultaneously for the two grabbed points ($W(S_L) = E_L$, $W(S_R) = E_R$) and produces a smooth warp in the vicinity of the grabbed points. The decay function takes as parameter the distance between a surface point P and the grabbed point O_L (left hand grab) or O_R (right hand grab). To design such a warp, a left motion that maps the grabbed pose S_L to the current

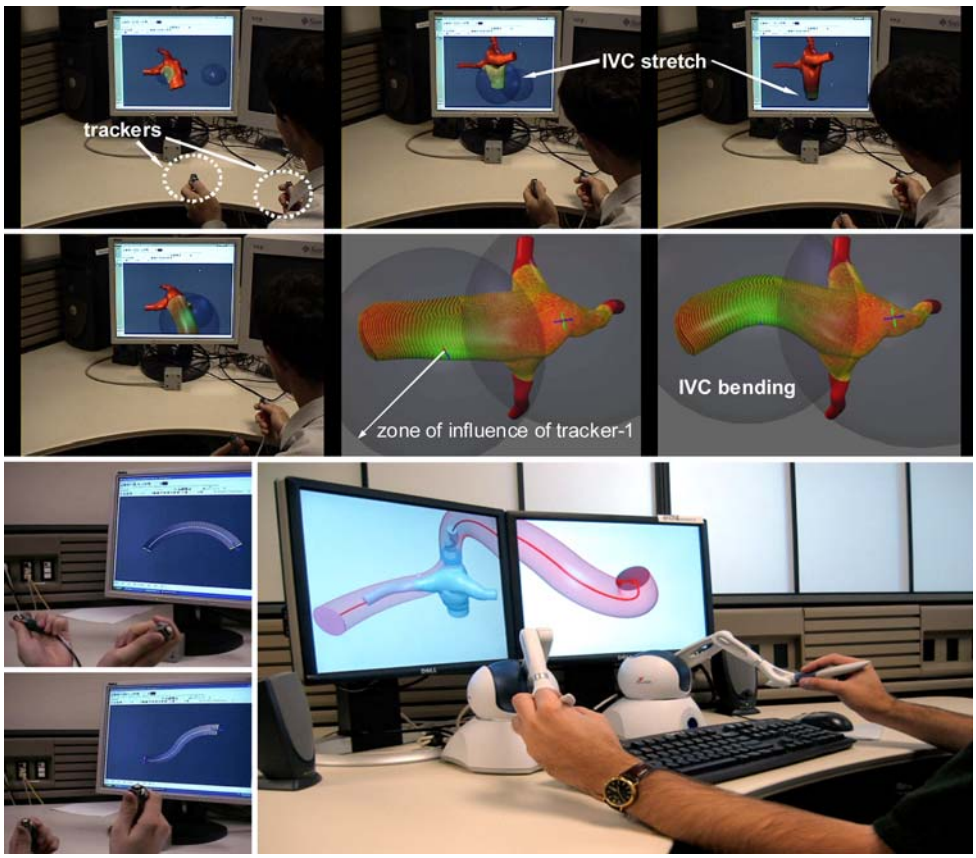

Fig. 2 Snapshots from the operation of interactive anatomical surface modification tool for surgical planning and communication. With the use of 3D magnetic trackers the inferior vena cava (IVC) of an intra-atrial model is modified (extension and bend) before exporting the modified geometry to the CFD analysis. The Bender tool operation is also illustrated without an anatomical model in the scene (two lower left corner pictures)

or end pose E_L and a right motion that maps S_R to E_R is computed. Then, a fraction of each motion is applied to all points of the shape that fall within the region of influence. The fraction between 0 and 1 is provided by the decay function. The decay function of a single hand is radial (i.e., a function of the distance to the grabbed point). To ensure a smooth transition cosine square function is chosen as the decay profile.

When the button is released, the deformation is frozen and the user may proceed to the next free-form surface modification operation.

After experimenting with a variety of motions that interpolate the starting and ending poses, it has been concluded that the screw motion (rigid body motion, L) provides the most intuitive deformations and leads to real-time performance. Using a screw motion has many advantages. A minimal screw motion between S and E minimizes rotation angle and translation distance, and is independent of the choice of the coordinate system and of the trajectory used to define S and E. The screw motion combines a rotation by angle b around an axis through point A parallel to vector K with a translation by dK. The parameters K, b, d, and A of such a screw motion may be computed quickly.

Let the grab pose be defined as $[O, I, J, K]$ by the grabbed point O and the orthonormal coordinate system $[I, J, K]$. The release pose is defined as $[O', I', J', K']$. For simplicity, assume that the cross-product $(I' - I) \times (J' - J)$ is not a null vector. (If it is, simultaneously permute the names in $[I, J, K]$ and $[I, J, K]$. If all permutations yield a null vector, the screw is a pure translation.) Then perform the following sequence of geometric constructions:

$$\begin{aligned} K &:= (I' - I) \times (J' - J) \\ K &:= K/\|K\| \\ b &:= 2\ \sin^{-1}(\|I' - I\|/(2\|K \times I\|)) \\ d &:= K \cdot OO' \\ A &:= (O + O')/2 + (K \times OO')/(2\tan(b/2)) \end{aligned} \tag{1}$$

Applying a screw motion to the vertices of a model may be done in real-time (20 frames/s) for large models with thousands of vertices.

The effect of both hands is combined by adding the displacements of each region of influence (RoI) as shown in Fig. 3. Points in the RoI of both hands will be displaced by fractions of each screw. To produce a smooth and natural displacement in the common region and to guarantee that the six constraints imposed by each hand are satisfied, the RoIs are squashed so that each excludes the center of the other.

Extending the simple spherical RoI, other deformation elements are possible which are helpful for modifying

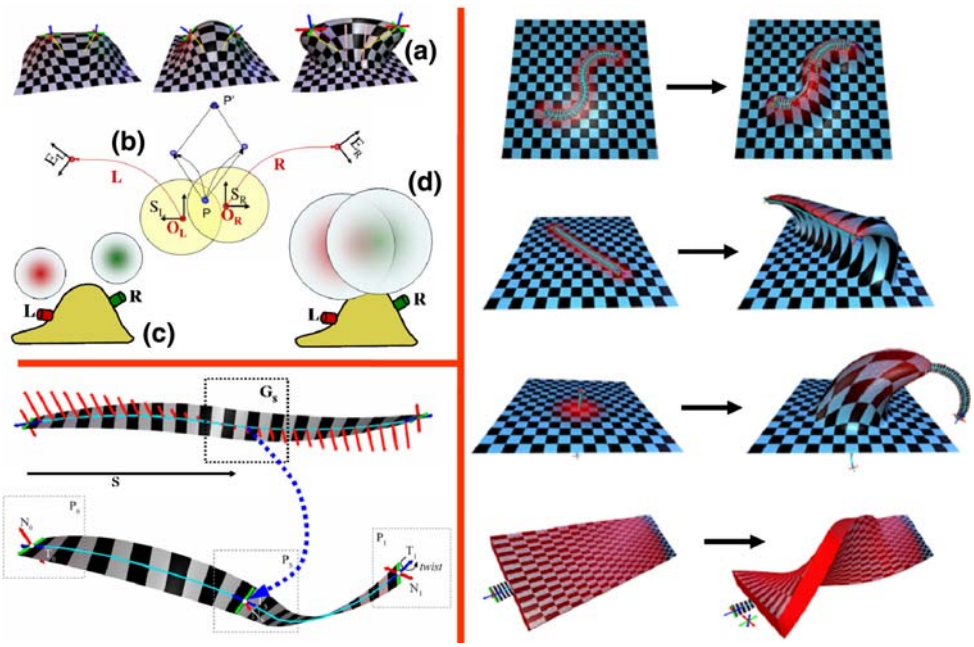

Fig. 3 *Top left* The two-hand warp for simultaneously deform a given shape. **a** Three instances from a basic two-hand warp operation. **b** Vector addition at the intersecting regions of influence. Distinct (**c**) and intersecting (**d**) regions of influence of the left and right hands. *Bottom left* the BENDER tool. Allowing surface deformations along an interactive curved ribbon of influence. *Right* surface features created with the BENDER tool

tubular surfaces or larger areas. The "Bender" tool simulates a flexible ribbon that is held by the user at both ends and may be moved, stretched, twisted and bent (Fig. 3). It can be positioned anywhere with respect to the model. When a button is pressed, the shape of the grabbed ribbon is captured. A deformation that maps it into the current ribbon (during editing) or the final ribbon (upon release) is computed.

The ribbon spine (central wire) is modeled using a smooth (i.e. tangent continuous) piecewise circular curve, as those used to model the spine of the baffle described in Sect. 3.2. The central wire of Bender is a single bi-arc curve, while the spine of the Baffle typically contains three control points and four circular arcs. Given the two end points P_0 and P_1 and the associated wire tangent directions T_0 and T_1, a bi-arc is computed as two smoothly connected circular arcs by computing a single scalar a satisfying the constraint $\|I_0 - I_1\|^2 = 4a^2$, where $I_0 = P_0 + aT_0$ and $I_1 = P_1 - aT_1$. The bi-arc is defined by the control polygon (P_0, I_0, I_1, P_1). The two arcs meet at $(I_0 + I_1)/2$, where they are both tangent to $I_1 - I_0$. Once the bi-arc is constructed, it may be parameterized. The twist is evenly distributed along the arc defining a parametric family of poses that interpolate the left and right hand poses controlled at the end of the bi-arc by the user. Compatible parameterizations of the initial (grab) and final (current or release) arcs defined by a mapping between corresponding poses. A screw motion is defined by each pair of corresponding poses.

The deformation maps each pose G_s of the grabbed ribbon into the corresponding pose P_s of the current ribbon (Fig. 3). A vertex of the model is deformed by one or two such screw motions, as discussed above for the two-handed FFD. To establish which screws are to be used and which decay weight is to be used, points on the bi-arc where the distance goes through a local minimum are computed. It can be proven that at most two such points exist. Once these points are identified, a one-screw or two-screw FFD is applied to the vertex. Examples of free-formed deformations created by this tool are shown in Fig. 3. Real-time video recordings of two anatomical editing and sculpturing sessions are presented [43, 57, 84, 85].

Snapshots of the first generation anatomical editing/sculpturing hardware and software implementation are shown in Fig. 2 as applied to the modification of an intraatrial total cavopulmonary connection (TCPC) anatomy. Two magnetic trackers allow 3D anatomical orientation and interactive deformation of the anatomy model with high efficiency and comfort. As the surgeon moves both hands, the arteries deform in real-time to follow the constraints defined by the displacement and orientation changes in both trackers. Zones of influences of the magnetic trackers are spherical. Their size can be adjusted interactively. The chosen shape modification can be frozen and easily exported to CFD analysis. Transfer of surface files between the in-house MRI image reconstruction tools and SURGEM is done via STL or Wavefront files. The resulting surfaces are then used to generate a grid for CFD studies. In order to provide the real-time response needed for the graphical feedback during direct manipulation, vessel material properties are not simulated. Instead, interactive operations allow the surgeon to quickly design the desired shapes that may reflect the outcome of a possible plan for the surgery while taking into account the

various spatial, physical, and operational constraints anticipated during surgery.

To understand the detailed 3D flow fields and evaluate the hemodynamic performance, patient-specific CFD studies are performed for the sample configurations that are virtually modified using SURGEM. Following the virtual anatomy editing stage, few additional operations are needed and all anatomies are directly meshed with the same parameters. Particular emphasis is given to achieve the same mesh density (finest mesh density) in all models to enable relative performance comparison. Details of the CFD analysis are available from earlier publications [47, 76, 77, 79]. Likewise, the details of magnetic resonance imaging (MRI) and phase contrast MRI 3D reconstruction protocols are also presented [12–14, 48, 68, 69, 77].

Quantifying the interactive geometric modifications in anatomical designs is required to associate the hemodynamic performance with original geometrical form. We developed an in-house iterative skelitalization routine where centerline and normal cross-sectional areas can be computed along the vessel segments for comparison between template designs [26, 27]. Automated interaction of these modules is possible through standardized file formats and will be implemented in future communications.

3 Selected applications

3.1 Anatomical sculpturing—free-form lumen surface deformations

The anatomical sculpturing and editing feature of the interactive surgical design tool is applied to three patient-specific 3D reconstructions. Several free-formed modifications are easily generated and sample resulted geometries are presented in Fig. 4. Unit sculpturing operations simulate inclusion of autologous tissue patches to construct desired size of flares, removal of the connection pouch, addition of various flares at LPA/RPA and IVC, dilation of RPA/LPA branch stenosis, modifications on the vessel confluence and generating alternative caval flow directions for selective left and right lung perfusion.

As a comparison in our earlier studies, we realized two of these modifications in the computer using the traditional commercial CAD software (1) removal severe LPA stenosis due to aortic arch reconstruction [47] and (2) reorientation of IVC-to-LSVC offset in dual SVC cases [79]. For the first case, a virtual pulmonary artery (PA) angioplasty was performed, while, in the second case, the IVC was shifted towards the center of the connection, hoping for a better perfusion at the PA segment bounded by the two SVCs. Modified and original anatomies were run in CFD and their performances are compared. For both cases, the virtual modifications brought in significant improvements in lung perfusion, cardiac output and cardiac energy loss. While both of our earlier anatomy editing operations were conceptually and geometrically simple (uniform dilatation and linear IVC translation), realizing these in the computer medium with the state-of-the art commercial CAD systems, introduced enormous difficulties. Each of these modifications required two to three weeks of manual anatomy editing using a combination of commercial CAD software. In contrast, several more complex anatomical modifications performed using SURGEM took only about 10 min and realized routinely, in a single interactive session. User times for unit operations and hemodynamic CFD performance predictions of these modified anatomies are presented in Table 1.

3.2 Interactive baffle creation and registration from surgical sketches

Congenital heart defects are surgically repaired through a series of palliative operations [42]. The final stage surgical operation involves the connection of IVC vessel to PA through an end-to-side anastomosis. Either an autologous partial conduit (intra-atrial) or a uniform diameter PTFE baffle (extra-cardiac) is used in this connection. Exact location and size of this conduit is determined at the time of the open heart surgery and require anatomy specific customization, trial-and-error. Left to surgeon's expertise this approach can extend the cardiopulmonary bypass time which can cause injury to vital organs (the brain, kidneys, lungs, and heart)—a problem seen in up to 30% of post-operative pediatric patients.

Upon requests from the surgeons, new functionality was introduced to SURGEM, to facilitate the computer aided construction of uniform diameter IVC baffle, which can be interactively modified as desired and located in the 3D space, by holding each end of the baffle with one hand and moving and bending them into the proper shape. The virtual IVC baffle is a circular cross-section tube whose spine (central axis) is represented by piecewise circular curve [56], a space curve made by smoothly joined circular arcs. Hence, the baffle is composed of smoothly abutting sections of tori. The user may grab, pull, bend, and twist the ends of the baffle or any junction between consecutive arcs. Furthermore, arcs may be split to provide local editing flexibility (See Sect. 2 for numerical details).

Three pediatric cardiac surgeons provided their surgical sketches of the IVC baffle construction for a given Glenn stage (pre-surgery anatomy) reconstruction. Reconstruction information that is passed to the surgeons also included the MRI images of the land mark anatomies such as the IVC, pulmonary veins, aorta and the heart. These sketches were

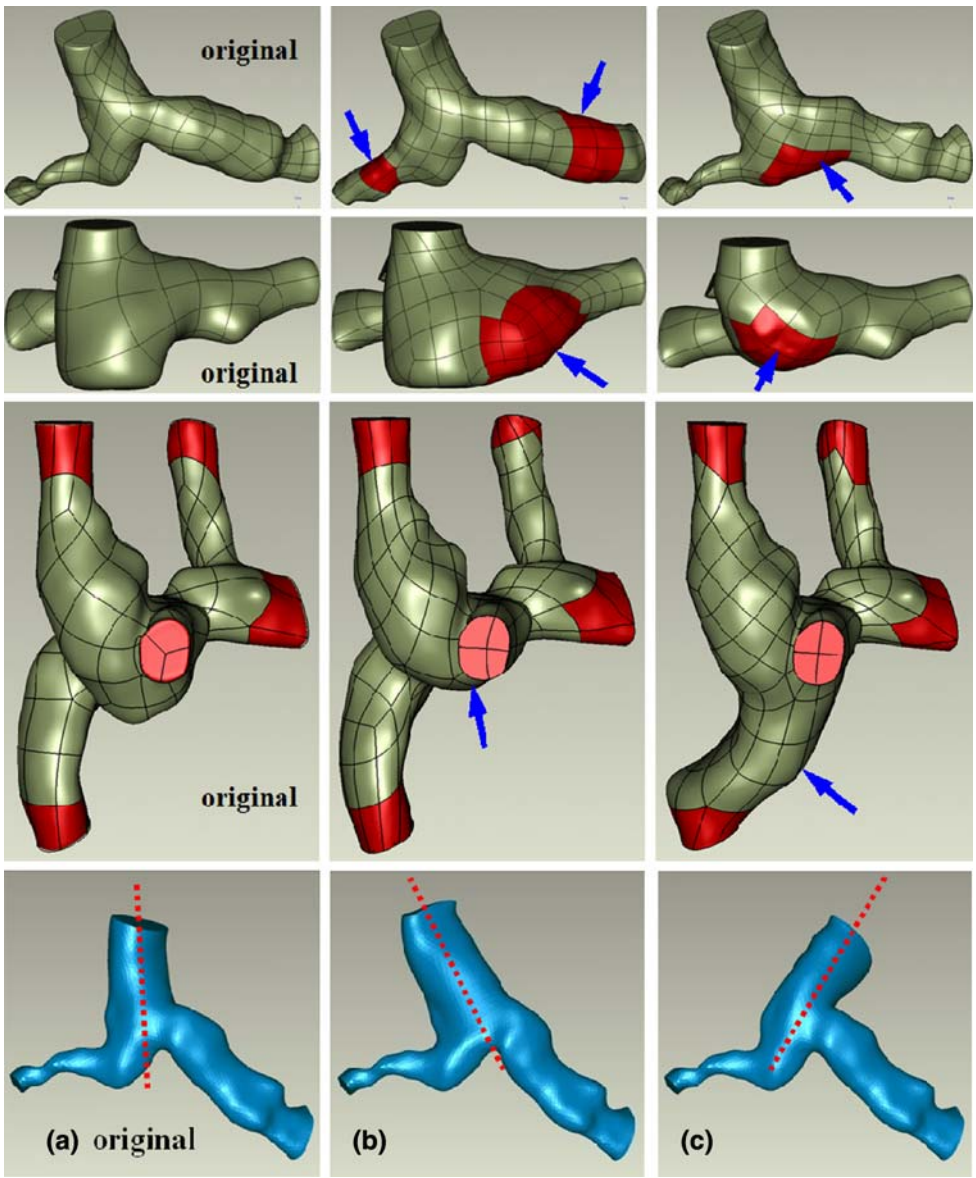

Fig. 4 Three patient-specific models (*left column*) and their selected free-formed deformed modifications generated using the interactive surgical design tool. Interactive anatomical changes are pointed by arrows, which include removal of the connection pouch, addition of various flares at LPA/RPA and IVC, dilation of RPA/LPA branch stenosis, modifications on the vessel confluence and generating alternative caval flow directions for selective left and right lung perfusion (*last row*)

turned into 3D models with SURGEM (Fig. 5), and saved for future comparative CFD analysis studies. Virtual anatomy design also enabled the construction of the IVC baffle in different diameters for the fixed 3D orientation to assess the fluid dynamic benefit of using larger conduits. Once the shape and orientation of the interactive baffle is decided final merging operation is performed manually using Geomagics [81]. This manual operation requires approximately 30 min per anatomical design. Samples of resulting anatomies (total 9) are summarized in Fig. 5.

To determine the user design cycle time for another anatomy all the surgically relevant morphologies including exact 3D reconstructions of pulmonary veins, IVC, heart and aorta are reconstructed from MRI and exported to SURGEM as separate objects (or layers; Fig 6). These additional anatomical structures precisely define the surgical constraints encountered intra-operatively. For this case creation of seven candidate surgical anatomies took $\sim$10 min for an inexperienced user using SURGEM. Model transparency and color coding of different anatomical layers was sufficient to identify the overlapping structures and enabled surgical planning conformal to the given patient specific 3D anatomical landmarks.

3.3 Pre-surgical patch size estimation

Using SURGEM, any vessel region of the final candidate anatomy can be interactively marked to identify the sections requiring surgical patches, suture lines or conduits and their geometrical properties can be calculated. These highlighted regions can also be exported as standalone

Table 1 Anatomical design cycle times reported for the common surgical operations encountered in the complex pediatric reconstructive surgeries

Case	Description	User Time
Ref. [47]	Virtual dilatation of single local LPA stenosis using conventional CAD tools (Ideas, ProE and Geomagics)	~3 weeks
Ref. [6]	IVC vessel cut, translate and merge with the rest of the anatomy (Ideas, ProE and Geomagics)	~2 weeks
Fig. 4	Anatomical sculpturing; local vessel dilatation, vessel redirection, flare, pouch design. For single unit design operation. (SURGEM)	<10 s
Fig. 7	Interactive analysis of surgical patch geometric properties (SURGEM)	<5 s
Fig. 5	3D IVC reconstructions of surgical sketches provided by the pediatric cardiac surgeon and merging with the rest of the anatomy (SURGEM + Geomagics)	~10 min
Fig. 6	Surgical TCPC baffle design for the given surgical constraints; Aorta and veins. Including merging with the rest of the anatomy (SURGEM + Geomagics)	~11 min

User times are for relatively inexperienced users and reported for unit anatomical operations and for "computational mesh generation ready" models. Relatively longer times reported for the last two rows is due to the merging operations performed using a general purpose commercial CAD system. For these cases operations performed in SURGEM took ~30 s and ~1 min, respectively

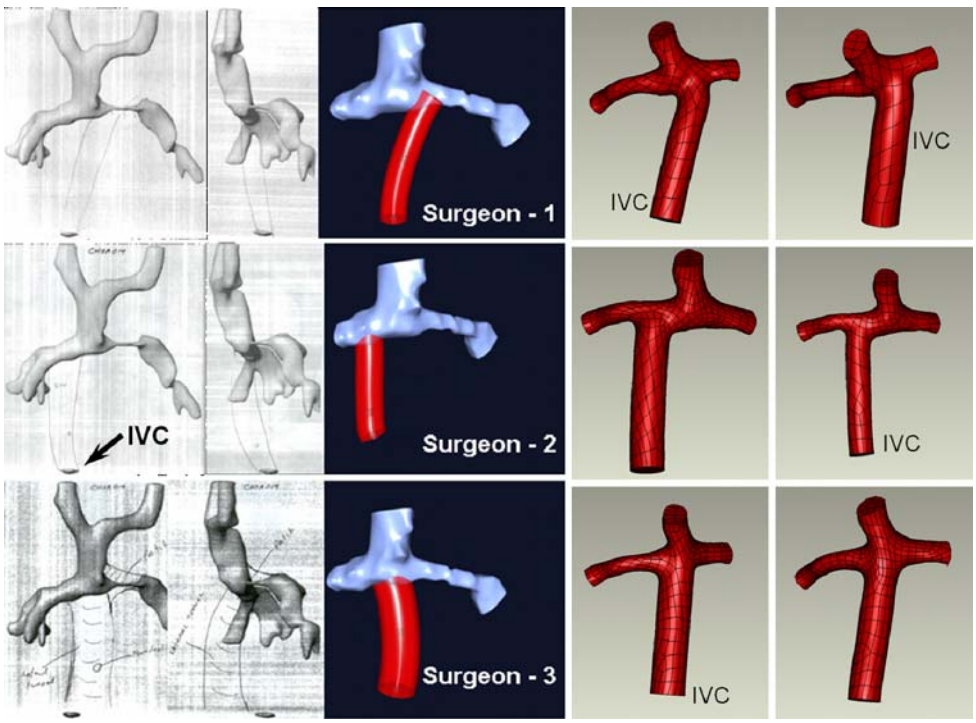

Fig. 5 *Left* IVC baffle configurations sketched by three pediatric cardiac surgeons in sagital and coronal views. *Middle* column is the 3D reconstructions of each design virtually in the computer by the surgical planning tool. On the *right*, the patient specific configurations with different IVC locations and cross-sectional diameters are presented. Final merging is completed using commercial modeling tools (six out of nine candidate models are shown)

surfaces for further specific analysis and development plan estimation (Fig. 7). For example, during pediatric cardiac surgeries intra-operative estimation of the size of a Dacron patch to be sutured requires trial-and-error even for an experienced surgeon. Pre-surgical development plan of the patch size calculated with SURGEM and compensated for vessel deformation will be potentially useful for the surgeon at the operating room to reduce cardiopulmonary bypass time considerably.

4 Hemodynamic performance and flow structures

Flow streamlines and velocity magnitudes calculated by the steady CFD simulations of a typical Glenn type pre-surgical anatomy and its virtual modifications are plotted in Fig. 8 (five candidate models are labeled A–E). Hydrodynamic power losses for different physiological operating points are calculated from CFD for each of these candidate designs and the extend of virtual geometrical modifications quantified by

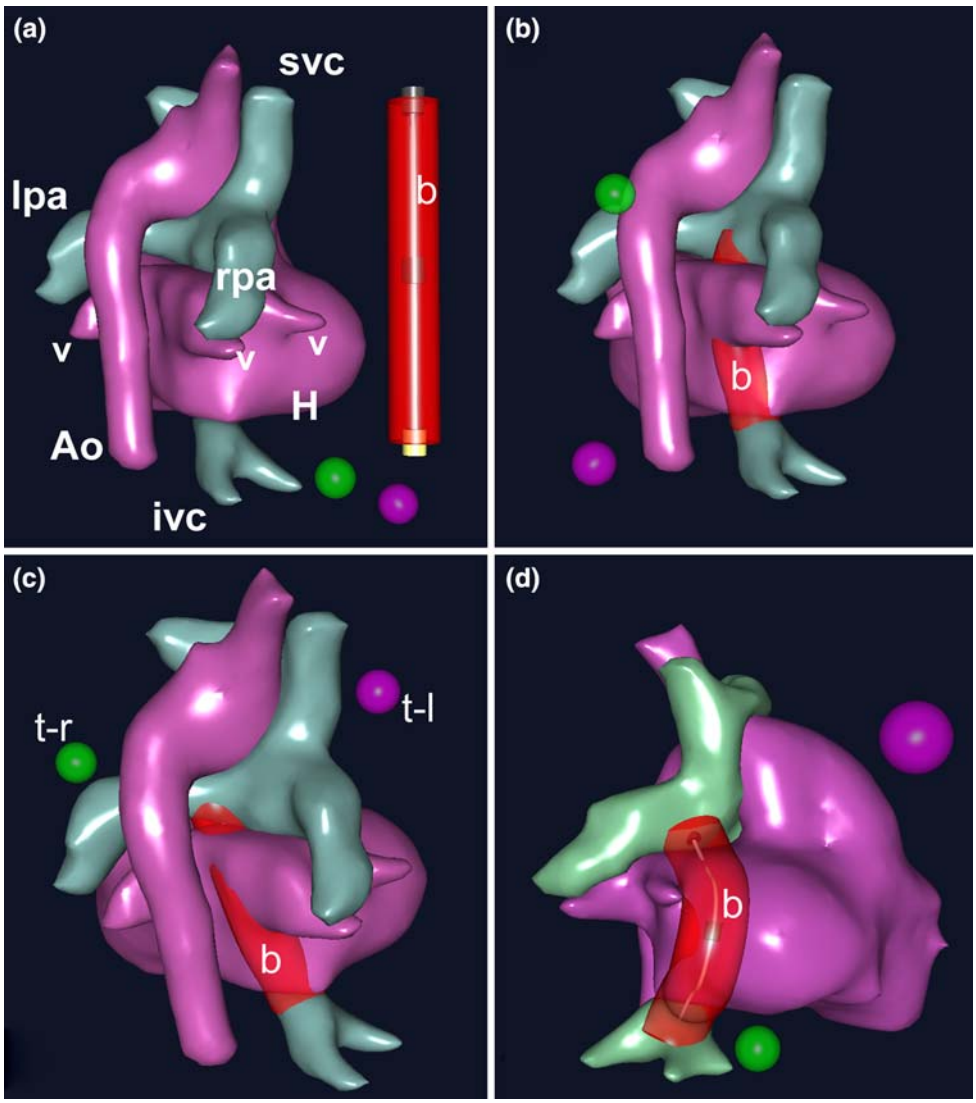

Fig. 6 A realistic pre-surgical planning scenario and the design of three candidate anastomosis configurations (**b** and **c** intra-atrial, **d** extra cardiac baffle, [77]). All critical surgical constraints are reconstructed in 3D; heart (h), aorta (Ao), pulmonary veins (v), inferior vena cava (ivc) and the pre-surgical Glenn (lpa, rpa, svc). Original configuration with un-deformed baffle (*b*) plotted in *red color* is shown in (**a**). Two intra-atrial connections are created one towards left lung (**c**) and the other towards the SVC, creating zero caval offset (**b**). The trackers used for editing operations are labeled with *t-r* and *t-l* corresponding to two hands

the skelitalization tool are reported elsewhere [49]. From these results it is observed that anatomical modification of the confluence region, model A, and inclusion of a proximal flare located upstream of the stenosis at the RPA, model D, produced minor effects in hydrodynamic power loss values. However, compared to the original anatomy, flow structures and flow streamline patterns were significantly different in the free-form designed flare and confluence. This is due to the fact that low flow velocities are encountered within the connection region and relatively uniform flow of the simple T-shape pathway. On the other hand, progressive dilatation of the multiple-stenosis located at left and right pulmonary arteries reduced power losses considerably $\sim$86%, as expected [21, 47].

Free-form anatomical modifications made in the pouch region of a hemi-Fontan type patient specific anatomy demonstrated similar results (Fig. 8) (Models G and H). Even drastic changes created at the pouch and LPA flare regions have not lead to any significant changes in the overall power loss values. These studies suggests that while flaring and connection design is critical for the "+" shaped final surgical reconstructions [21, 47] (as they change the vortex interaction in opposing IVC and SVC streams), these features influence the hydrodynamic power losses relatively less for second stage TCPC pathways. High power losses originated at the pulmonary branches are further augmented by the secondary flows generated due to turning SVC flow. CFD analysis of the extracardiac anatomy presented in Fig. 6d is also performed and plotted in Fig. 8. Other anatomical configurations created using SURGEM could be analyzed similarly.

5 Discussion

A state-of-the-art patient specific analysis methodology is developed integrating all technologies including, PC-MRI and MRI 3D reconstruction, grid generation, experimental

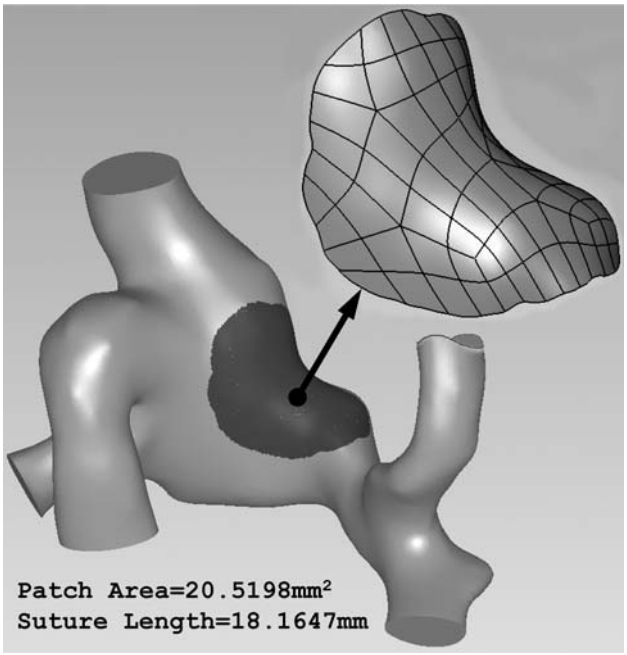

Fig. 7 The surgical patch is interactively highlighted with red color using magnetic trackers on the complex anatomy which is then exported as a standalone lumen surface for further analysis. For this example suture length and the area of the autologous patch that will be needed during surgery is calculated

validation, CFD analysis and post-processing. Recent advances in patient-specific analysis protocols allow the fast hemodynamic performance analysis of a given anatomy with fixed morphology routinely, for a hundreds of models [3]. The missing links that have emerged are surgical planning, 3D reconstruction and morphological design. This involves creation of alternative anatomies and manipulation of anatomies that are changing, either by the user, interactively or during an automated optimization process of inverse design. Similarly vascular growth and development involve a complex series of morphological changes, which can be analyzed and represented robustly with the presented bio-CAD approach [50]. Models with anatomical variations are also needed for verification tests of computational models. For example, in CFD model verification studies, families of anatomical models are routinely needed to test the effects of inlet vessel pathway shape on the patient specific CFD results [43]. Furthermore, registration of a medical device (like an aortic canulla [48], mechanical valve, assist device [57] or a stent [86]) with respect to a given complex patient-specific anatomy is occasionally required for computational modeling. Creation of such alternative morphologies and complex anatomical design/registration operations could become considerably more straightforward with the tools presented in this paper. The proposed tools are expected to be useful in other biomedical applications that are even more complex than pediatric cardiac surgeries. These include mitral valve repair [78] and ventricle reconstruction surgeries [58] to name a few. Additionally, the strong dependence of the presented methods on imaging technology ensures that the efficacy of these methods will only continue to improve as the technological capabilities of imaging mediums such as MRI progress.

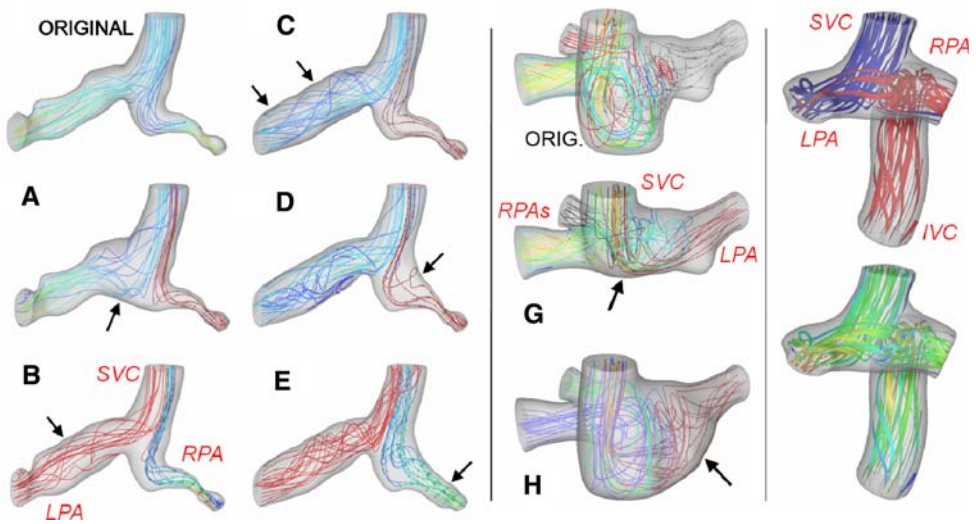

Fig. 8 3D CFD flow fields of candidate free-form deformed anatomical models. Interactive local modifications made by the user sequentially and are highlighted with arrows. **a** New confluence design; **b**, **c** RPA branch modifications; **d** LPA flare design; **e** LPA stenosis dilatation. Colors represent velocity magnitudes (*red*, high- and *blue* colors correspond to low values). **g** Effects of removing the Hemi-Fontan pouch; **h** LPA branch flare design. On the *right* streamlines for the extra-cardiac baffle configuration of Fig. 6, Case **d** is plotted

Patient-specific methodologies promise to be of value in clinical practice and in surgical decision making. However, their deployment has been hampered by the cost of designing the 3D models of the modified anatomies. This cost has been excessive, because traditional CAD models, which have been used for this task, do not provide support for specifying the desired anatomical variation of 3D geometric models of the complexity of a cardiovascular system. Using SURGEM design cycle times are considerably shorter compared to the earlier reported user experience as presented in Table 1. The improvements in the anatomical design cycle are significant and allowed routine hemodynamic analysis of larger number of candidate models.

Our interactions with cardiac surgeons and cardiologists identified the key technologies that need to be further developed and integrated in to SURGEM. These future improvements are prioritized as follows:

(1) Enabling fully automated merging of the created baffle with the pre-surgery anatomy and clean-up.
(2) Inclusion of vessel wall thickness to the geometrical models.
(3) Development of specific patch augmentation and virtual balloon angioplasty tools—an improved local vessel dilatation tool for virtual repair of stenosed vessels.
(4) Preparation of a standard graft database which includes a selection of standard grafts to be used during the IVC vessel reconstruction.
(5) Additional helpful editing and bookkeeping features: (a) a local measurement tool of diameters, distances, areas marked areas of the vessel surface; (b) introducing vessel labels; (c) selective use of colors and transparency for identifying different materials; veins, arteries, grafts; (d) on vessel lumen drawing of surgical marks for identifying the anastomosis lines; (e) marking selected regions of the anatomy as stationary and locking these regions to avoid any accidental changes (the inlet/outlet surfaces should be smooth and planar for finite-element analysis. Lock these regions as stationary to keep their shape constant); (f) streamlined data export to computational fluid dynamics analysis.
(6) Automated generation of a family of vessel anatomies as a function of the single geometric parameter such as the generator curve arc-length in between the two given start and end locations to be used in parametric optimization studies.
(7) As most surgical reconstructions are created on cardiopulmonary bypass without blood flow, the geometric shape should be assessed and visualization in the post-bypass hydrostatic loading condition needs to be provided. This task requires coupling SURGEM with the finite element analysis [17]. Currently, it is implicitly assumed that the surgeon can incorporate this effect based on his/her experience.

Advanced patient-specific analysis techniques could potentially be useful in the clinical evaluation of complex patient hemodynamics. Increases in the efficiency and robustness associated with this type of analysis will eventually enable assessment of the predictive value of CFD simulation in clinical practice through prospective testing in large numbers of patients before and after intervention. Next-generation biological computer aided shape design tools that are founded on advanced geometry processing and specifically developed for arbitrary, time-varying, complex/flexible cardiovascular anatomies enable virtual cardiovascular surgeries efficiently and provide an alternative environment for patient-specific and custom virtual surgeries. Besides providing quantitative pre-surgery functional assessment of the intended operation, these tools may also be useful for surgical training and for innovating new technologies and techniques for treatment in the computer medium. Robust complex geometry handling capability will allow the surgeon, cardiologist or the biomedical engineer to interact with the anatomy, propose changes, quantify them and test their effect.

6 Conclusion

The shape modifications produced during surgical operations are closer to those a sculptor would envision. To model their effect, the user must have total control over an intuitive and powerful human–shape interface. The anatomy editing approach presented here is applied to a large number of patient specific pediatric cardiac anatomies having complex topologies. On a total of eight different patient specific anatomies more than 30 new anatomical designs (or candidate configurations) are created in this study. This approach is found to be practical for applications that require hemodynamic exploration and identification of the specific anatomical features influencing the performance. User times indicate significant improvements over the existing traditional CAD systems. Anatomical design methodology is further integrated to the patient specific CFD analysis. Virtual surgical prediction tools that aid the surgical decision making process once clinically implemented will reduce the CPB time, improve hemodynamic outcome and eliminate trial-error during complex cardiac surgeries.

Acknowledgments Drs. Mark Fogel, William Gaynor at the Children's Hospital of Philadelphia, Dr. Pedro del Nido, Boston Children's Hospital, Paul Krishborn-Emory University and Dr. W. James Parks at

Sibley Heart Center, Egleston Children's Hospital/Emory University, Atlanta. We also thank Hiroumi Kitajima and undergraduate student Gopinath Jayaprakash for providing most of the reconstructions used in this study. Also Paymon Nourparvar and Vasu Yerneni assisted in the CFD simulations through Georgia Tech President's Undergraduate Research Awards (PURA). Financial support: National Heart, Lung and Blood Institute Grant HL67622 and Seed Grant from the Graphics Visualization and Usability (GVU) Center at Georgia Tech.

References

1. Barnett GH (1999) The role of image-guided technology in the surgical planning and resection of gliomas. J Neurooncol 42(3):247–258
2. Barnett GH, Miller DW, Weisenberger J (1999) Frameless stereotaxy with scalp-applied fiducial markers for brain biopsy procedures: experience in 218 cases. J Neurosurg 91(4):569–576
3. Cebral JR, Castro MA, Burgess JE, Pergolizzi RS, Sheridan MJ, Putman CM (2005) Characterization of cerebral aneurysms for assessing risk of rupture by using patient-specific computational hemodynamics models. Am J Neuroradiol 26(10):2550–2559
4. Cheutet V, Catalano C, Pernot J, Falcidieno B, Giannini F, Leon J (2005) 3D sketching for aesthetic design using fully free-form deformation features. Comput Graph 29(6):916–930
5. de Zelicourt DA, Pekkan K, Wills L, Kanter K, Forbess J, Sharma S, Fogel M, Yoganathan AP (2005) In vitro flow analysis of a patient-specific intraatrial total cavopulmonary connection. Ann Thorac Surg 79(6):2094–2102
6. de Zelicourt DA, Pekkan K, Parks J, Kanter K, Fogel M, Yoganathan AP (2006) Flow study of an extracardiac connection with persistent left superior vena cava. J Thorac Cardiovasc Surg 131(4):785–791
7. Deleval MR, Kilner P, Gewillig M, Bull C (1988) Total cavopulmonary connection—a logical alternative to atriopulmonary connection for complex Fontan operations—experimental studies and early clinical-experience. J Thoracic Cardiovasc Surg 96(5):682–695
8. Dubini G, Migliavacca F, Pennati G, de Leval MR, Bove EL (2004) Ten years of modelling to achieve haemodynamic optimisation of the total cavopulmonary connection. Cardiol Young 14(Suppl 3):48–52
9. Duncan J (1989) Computer-aided sculpture. Cambridge University Press, London
10. Ensley AE, Lynch P, Chatzimavroudis GP, Lucas C, Sharma S, Yoganathan AP (1999) Toward designing the optimal total cavopulmonary connection: an in vitro study. Ann Thorac Surg 68(4):1384–1390
11. Fang X, Bao H, Pheng A, Tien T, Peng Q (2001) Continuous field based free-form surface modeling and morphing. Comput Graph 25(2):235–243
12. Frakes DH, Conrad CP, Healy TM, Monaco JW, Fogel M, Sharma S, Smith MJ, Yoganathan AP (2003) Application of an adaptive control grid interpolation technique to morphological vascular reconstruction. IEEE Trans Biomed Eng 50(2):197–206
13. Frakes DH, Smith MJ, Parks J, Sharma S, Fogel SM, Yoganathan AP (2005) New techniques for the reconstruction of complex vascular anatomies from MRI images. J Cardiovasc Magn Reson 7(2):425–432
14. Frakes DH, Dasi LP, Pekkan K, Kitajima HD, Sundareswaran K, Yoganathan AP, Smith MJ (2008) A new method for registration-based medical image interpolation. IEEE Trans Med Imaging 27(3):370–377
15. Gildenberg PL, Labuz J (2006) Use of a volumetric target for image-guided surgery. Neurosurgery 59(3):651–659 discussion 651–659
16. Giordana S, Sherwin SJ, Peiro J, Doorly DJ, Crane JS, Lee KE, Cheshire NJ, Caro CG (2005) Local and global geometric influence on steady flow in distal anastomoses of peripheral bypass grafts. J Biomech Eng 127(7):1087–1098
17. Gu H, Chua A, Tan B, Hung K (2006) Nonlinear finite element simulation to elucidate the efficacy of slit arteriotomy for end-to-side arterial anastomosis in microsurgery. J Biomech 39(3):435–443
18. Hui K (2003) Free-form deformation of constructive shell models. Comput Aided Des 35(13):1221–1234
19. Hunter KS, Lanning CJ, Chen SY, Zhang Y, Garg R, Ivy DD, Shandas R (2006) Simulations of congenital septal defect closure and reactivity testing in patient-specific models of the pediatric pulmonary vasculature: a 3D numerical study with fluid-structure interaction. J Biomech Eng 128(4):564–572
20. Jackson MJ, Bicknell CD, Zervas V, Cheshire NJ, Sherwin SJ, Giordana S, Peiro J, Papaharilaou Y, Doorly DJ, Caro CG (2003) Three-dimensional reconstruction of autologous vein bypass graft distal anastomoses imaged with magnetic resonance: clinical and research applications. J Vasc Surg 38(3):621–625
21. Kanter K, Krishnankutty RR, Dasi L, Kitajima H, Pekkan K, Fogel M, Witehead K, Sharma S, Yoganathan A (2008) Total cavopulmonary connection efficiency: importance of pulmonary artery diameter. J Thoracic Cardiovasc Surg (in press)
22. Kasik D, Buxton W, Ferguson D (2005) Ten CAD challenges. IEEE Comput Graph Appl 25(2):84–92
23. Kim J, Rossignac J (2000) Screw motions for the animation and analysis of mechanical assemblies. Int J Jpn Soc Mech Eng 44(1):156–163
24. Kim B, Rossignac J (2003) Collision prediction for polyhedra under screw motions. ACM Symp Solid Model Appl, pp. 4–10
25. Komerska R, Ware C (2004) Haptic state–surface interactions. IEEE Comput Graph Appl 24(6):52–59
26. Krishnankutty R, Dasi LP, Pekkan K, Sundareswaran KS, Fogel M, Sharma S, Kanter K, Yoganathan AP (2008) Quantitative analysis of extra-cardiac vs intra-atrial Fontan anatomic geometries. Ann Thoracic Surg 85(3):810–817
27. Krishnankuttyrema R, Dasi L, Pekkan K, Sundareswaran K, Kitajima H, Yoganathan AP (2007) A unidimensional representation of the total cavopulmonary connection. In: ASME 2007 summer bioengineering conference (SBC2007), ASME, Keystone Resort and Conference Center, Keystone
28. Kurodaa Y, Nakaob M, Kurodac T, Oyamad H, Komorie M (2005) Interaction model between elastic objects for haptic feedback considering collisions of soft tissue. Comput Methods Programs Biomed 80:216–224
29. Laks H, Ardehali A, Grant PW, Permut L, Aharon A, Kuhn M, Isabel-Jones J, Galindo A (1995) Modification of the Fontan procedure. Superior vena cava to left pulmonary artery connection and inferior vena cava to right pulmonary artery connection with adjustable atrial septal defect. Circulation 91(12):2943–2947
30. Lanning C, Chen SY, Hansgen A, Chang D, Chan KC, Shandas R (2004) Dynamic three-dimensional reconstruction and modeling of cardiovascular anatomy in children with congenital heart disease using biplane angiography. Biomed Sci Instrum 40:200–205
31. Li Z, Kleinstreuer C (2005) Fluid–structure interaction effects on sac-blood pressure and wall stress in a stented aneurysm. J Biomech Eng 127(4):662–671
32. Li Z, Kleinstreuer C (2006) Effects of major endoleaks on a stented abdominal aortic aneurysm. J Biomech Eng 128(1):59–68
33. Lin Y, Wang C, Dai K (2005) Reverse engineering in CAD model reconstruction of customized artificial joint. Med Eng Phys 27(2):189–193

34. Linte C, Wierzbicki M, Moore J, Guiraudon G, Jones D, Peters T (2007) On enhancing planning and navigation of beating-heart mitral valve surgery using pre-operative cardiac models. In: 29th IEEE EMBS annual international conference, Lyon
35. Llamas I, Kim B, Gargus J, Rossignac J, Shaw C (2003) Twister: a space-warp operator for the two-handed editing of 3D shapes. In: Proceeding ACM SIGGRAPH, p 663
36. Llamas I, Powell A, Rossignac J, Shaw CD (2005) Bender: a virtual ribbon for deforming 3D shapes in biomedical and styling applications. In: ACM symposium on solid modeling and applications, pp 89–99
37. Mackerle J (2004) Finite element modelling and simulations in dentistry: a bibliography 1990–2003. Comput Methods Biomech Biomed Eng 7(5):277–303
38. Mario R (2006) Polygonal modeling: basic and advanced techniques. Wordware Pub, Plano
39. Migliavacca F, de Leval MR, Dubini G, Pietrabissa R, Fumero R (1999) Computational fluid dynamic simulations of cavopulmonary connections with an extra-cardiac lateral conduit. Med Eng Phys 21:187–193
40. Migliavacca F, Kilner PJ, Pennati G, Dubini G, Pietrabissa R, Fumero R, de Leval MR (1999) Computational fluid dynamic and magnetic resonance analyses of flow distribution between the lungs after total cavopulmonary connection. IEEE Trans Biomed Eng 46(4):393–399
41. Migliavacca F, Dubini G, Bove E, de Leval M (2003) Computational fluid dynamics simulations in realistic 3-D geometries of the total cavopulmonary anastomosis: the influence of the inferior caval anastomosis. J Biomech Eng 125(6):805–813
42. Mitchell ME, Ittenbach RF, Gaynor JW, Wernovsky G, Nicolson S, Spray TL (2006) Intermediate outcomes after the Fontan procedure in the current era. J Thoracic Cardiovasc Surg 131(1):172–180
43. Moyle K, Antiga L, Steinman D (2006) Inlet conditions for image-based CFD models of the carotid bifurcation: is it reasonable to assume fully developed flow? J Biomech Eng 128(3):371–379
44. Murakami H, Yoshimura N, Kitahara J, Otaka S, Ichida F, Misaki T (2006) Collision of the caval flows caused early failure of the Fontan circulation. J Thorac Cardiovasc Surg 132(5):1235–1236
45. Pekkan K, ZD, Sorensen D, Kitajima H, Yoganathan AP (2005) Surgical planning of the total cavopulmonary connection using MRI, computational and experimental fluid mechanics. In: 3rd European medical and biological engineering conference, EMBEC Prague, Czech Republic
46. Pekkan K, Frakes D, De Zelicourt D, Lucas CW, Parks WJ, Yoganathan AP (2005) Coupling pediatric ventricle assist devices to the Fontan circulation: simulations with a lumped-parameter model. Asaio J 51(5):618–628
47. Pekkan K, Kitajima HD, de Zelicourt D, Forbess JM, Parks WJ, Fogel MA, Sharma S, Kanter KR, Frakes D, Yoganathan AP (2005) Total cavopulmonary connection flow with functional left pulmonary artery stenosis—angioplasty and fenestration in vitro. Circulation 112(21):3264–3271
48. Pekkan K, Dur O, Kanter K, Sundareswaran K, Fogel M, Yoganathan A, Ündar A (2008) Neonatal aortic arch hemodynamics and perfusion during cardiopulmonary bypass. J Biomech Eng (in press)
49. Pekkan K, Krishnankutty R, Dasi L, Yerneni S, de Zélicourt D, Fogel M, Kanter K, Yoganathan A (2008) Hemodynamic performance of stage-2 univentricular reconstruction: Glenn vs. hemi-Fontan templates. Ann Biomed Eng (2nd review)
50. Pekkan K, Dasi LP, Nourparvar P, Yerneni S, Tobita K, Fogel MA, Keller B, Yoganathan A (2008) In vitro hemodynamic investigation of the embryonic aortic arch at late gestation. J Biomech 41(8):1697–1706
51. Perktold K, Hofer M, Rappitsch G, Loew M, Kuban BD, Friedman MH (1998) Validated computation of physiologic flow in a realistic coronary artery branch. J Biomech 31(3):217–228
52. Prosi M, Perktold K, Ding Z, Friedman MH (2004) Influence of curvature dynamics on pulsatile coronary artery flow in a realistic bifurcation model. J Biomech 37(11):1767–1775
53. Qin S, Wright D, Kang J, Prieto P (2005) Incorporating 3D body motions into large-sized freeform surface conceptual design. Biomed Sci Instrum 41:271–276
54. Raghavan ML, Kratzberg J, Castro de Tolosa EM, Hanaoka MM, Walker P, da Silva ES (2005) Regional distribution of wall thickness and failure properties of human abdominal aortic aneurysm. J Biomech 39(16):3010–3016
55. Rhoten RL, Luciano MG, Barnett GH (1997) Computer-assisted endoscopy for neurosurgical procedures: technical note. Neurosurgery 40(3):632–637 discussion 638
56. Rossignac J, Requicha A (1987) Piecewise-circular curves for geometric modeling. IBM J Res Dev 13:296–313
57. Saeed D, Ootaki Y, Noecker A, Weber S, Smith WA, Duncan BW, Fukamachi K (2008) The Cleveland clinic pedipump: virtual fitting studies in children using three-dimensional reconstructions of cardiac computed tomography scans. Asaio J 54(1):133–137
58. Sartipy U, Albage A, Lindblom D (2005) The Dor procedure for left ventricular reconstruction. Ten-year clinical experience. Eur J Cardio-thoracic Surg 27:1005–1010
59. Sheppard L (2005) Virtual surgery brings back smiles. IEEE Comput Graph Appl 25(1):6–11
60. Soerensen DD, Pekkan K, Sundareswaran KS, Yoganathan AP (2004) New power loss optimized Fontan connection evaluated by calculation of power loss using high resolution PC-MRI and CFD. Conf Proc IEEE Eng Med Biol Soc 2:1144–1147
61. Sorensen TS, Greil GF, Hansen OK, Mosegaard J (2006) Surgical simulation—a new tool to evaluate surgical incisions in congenital heart disease? Interact Cardiovasc Thorac Surg 5(5):536–539
62. Steele BN, Draney MT, Ku JP, Taylor CA (2003) Internet-based system for simulation-based medical planning for cardiovascular disease. IEEE Trans Inf Technol Biomed 7(2):123–129
63. Steele BN, Wan J, Ku JP, Hughes TJ, Taylor CA (2003) In vivo validation of a one-dimensional finite-element method for predicting blood flow in cardiovascular bypass grafts. IEEE Trans Biomed Eng 50(6):649–656
64. Steinman DA (2002) Image-based computational fluid dynamics modeling in realistic arterial geometries. Ann Biomed Eng 30(4):483–497
65. Steinman DA (2004) Image-based computational fluid dynamics: a new paradigm for monitoring hemodynamics and atherosclerosis. Curr Drug Targets Cardiovasc Haematol Disord 4(2):183–197
66. Steinman DA, Taylor CA (2005) Flow imaging and computing: large artery hemodynamics. Ann Biomed Eng 33(12):1704–1709
67. Steinman DA, Vorp DA, Ethier CR (2003) Computational modeling of arterial biomechanics: insights into pathogenesis and treatment of vascular disease. J Vasc Surg 37(5):1118–1128
68. Sundareswaran KS, KH, Pekkan K, Soerensen DD, Yerneni V, Parks WJ, Sallee D, Yoganathan AP (2005) Flow field comparison in reverse engineered total cavopulmonary connection anatomic models: high resolution PC MRI vs CFD. In: International society of magnetic resonance in medicine (ISMRM) 13th scientific meeting, Miami
69. Sundareswaran KS, Kanter KR, Kitajima HD, Krishnankutty R, Sabatier JF, Parks WJ, Sharma S, Yoganathan AP, Fogel M (2006) Impaired power output and cardiac index with hypoplastic left heart syndrome: a magnetic resonance imaging study. Ann Thoracic Surg 82(4):1267–1277

70. Sundareswaran KS, Pekkan K, Dasi LP, Kitajima HD, Whitehead K, Fogel MA, Yoganathan AP (2007) Significant impact of the total cavopulmonary connection resistance on cardiac output and exercise performance in single ventricles. Circulation 116(16_MeetingAbstracts), p 479
71. Sundareswaran KS, Pekkan K, Dasi LP, Whitehead K, Sharma S, Kanter K, Fogel MA, Yoganathan AP (2008) The total cavopulmonary connection resistance: a significant impact on single ventricle hemodynamics at rest and exercise. Am J Physiol (in press)
72. Testi D, Quadrani P, Petrone M, Zannoni C, Fontana F, Viceconti M (2004) JIDE: a new software for computer-aided design of hip prosthesis. Comput Methods Programs Biomed 75:213–220
73. van Dijk C, Mayer A (1997) Sketch input for conceptual surface design. Comput Ind 34(1):125–137
74. Vannier MW, Marsh JL (1996) Three-dimensional imaging, surgical planning, and image-guided therapy. Radiol Clin North Am 34(3):545–563
75. Varady T, Martin R, Cox J (1997) Reverse engineering of geometric models—an introduction. Comput Aided Des 29(4):255–268
76. Wang C, Pekkan K, de Zelicourt D, Horner M, Parihar A, Kulkarni A, Yoganathan AP (2007) Progress in the CFD modeling of flow instabilities in anatomical total cavopulmonary connections. Ann Biomed Eng 35(11):1840–1856
77. Whitehead KK, Pekkan K, Kitajima HD, Paridon SM, Yoganathan AP, Fogel MA (2007) Nonlinear power loss during exercise in single-ventricle patients after the Fontan: insights from computational fluid dynamics. Circulation 116(11 Suppl):I165–I171
78. Yacoub M, Cohn L (2004) Novel approaches to cardiac valve repair: from structure to function: part I. Circulation 109(8):942–950
79. Zélicourt D, Pekkan K, Parks WJ, Kanter K, Fogel M, Yoganathan AP (2006) Flow study of an extra-cardiac connection with persistent left superior vena cava. J Thoracic Cardiovasc Surg 131(4):785–791
80. Zeng D, Ding Z, Friedman MH, Ethier CR (2003) Effects of cardiac motion on right coronary artery hemodynamics. Ann Biomed Eng 31(4):420–429
81. 2008 Geomagics Studio. Geomagics Durham, NC, USA
82. 2008 Autodesk Maya. Autodesk, San Rafael, CA, USA
83. 2008 Video clip. http://a-lex.powelltown.com/BenderClipsSmall.mov
84. 2008 Video clip - 1. http://www.andrew.cmu.edu/user/kpekkan/chopb-short-full.avi
85. 2008 Video Clip - 2. http://www.andrew.cmu.edu/user/kpekkan/FastFontan.wmv
86. 2008 2nd Virtual Intracranial Stenting Challenge (VISC08). http://www.cilab.upf.edu/visc08/